

Charge density mapping of strongly-correlated few-electron two-dimensional quantum dots by scanning probe technique

E. Wach, D.P. Żebrowski, and B. Szafran

AGH University of Science and Technology,
Faculty of Physics and Applied Computer Science, al. Mickiewicza 30, 30-059
Kraków, Poland

Abstract. We perform a numerical simulation of mapping of charge confined in quantum dots by the scanning probe technique. We solve the few-electron Schrödinger equation with the exact diagonalization approach and evaluate the energy maps in function of the probe position. Next, from the energy maps we try to reproduce the charge density distribution using an integral equation given by the perturbation theory. The reproduced density maps are confronted with the original ones. The present study covers two-dimensional quantum dots of various geometries and profiles with the one-dimensional (1D) quantum dot as a limit case. We concentrate on large quantum dots for which strong electron-electron correlations appear. For circular dots the correlations lead to formation of Wigner molecules that in the presence of the tip appear in the laboratory frame. The unperturbed rotationally-symmetric charge density is surprisingly well reproduced by the mapping. We find in general that the size of the confined droplet as well as the spatial extent of the charge density maxima is underestimated for repulsive tip potential and overestimated for the attractive tip. In lower-symmetry quantum dots the Wigner molecules with single-electron islands nucleate for some electron numbers even in the absence of the tip. These charge densities are well resolved by the mapping. The single-electron islands appear in the laboratory frame provided that classical point charge density distribution is unique, in the 1D limit of confinement in particular. We demonstrate that for electron systems which possess a few equivalent classical configurations the repulsive probe switches between the configurations. In consequence the charge density evades mapping by the repulsive probe.

1. Introduction

Local properties of semiconductor nanostructures can be probed by the scanning gate microscopy [1] (SGM) in which the charge of the atomic force microscope tip perturbs the potential landscape below the surface of the semiconductor within the space occupied by confined charge carriers. SGM covers both the open systems (quantum point contacts [2], resonant cavities [3], quantum rings [4]) in which the probe is used to read out the wave function at the Fermi level from the conductance perturbations as well as systems that are weakly coupled to the reservoirs, i.e. closed quantum dots [6, 7, 8, 9, 11, 12, 13, 14, 15]. For the latter, the current flows through the quantum dot only outside the Coulomb blockade conditions [16], i.e., when the chemical potential ($\mu_N = E_N - E_{N-1}$) of N confined electrons lies within the transport window defined by the Fermi levels of source and drain. In experiments, the tip-induced variation of E_N is determined from the shift of voltages that is necessary for restoration of the current flow [6, 8, 9, 13]. Since the variation depends on the electron density beneath the tip this technique allows for visualization of the charge density [5]. The details of the variation of the charge density can be detected only for large quantum dots exceeding the range of tip potential. In large dots and at low electron densities the SGM technique can – at least potentially – resolve single-electron islands within the few-electron quantum dot which are formed as an effect of strong electron-electron correlations with the charge density nucleating to Wigner molecules [18, 19].

The effort on the extraction of the confined charge density by the scanning gate microscopy concerned mostly quasi one-dimensional (1D) quantum dots defined within a quantum wire [7, 9, 10, 11, 12, 14, 15]. Wigner molecules in 1D quantum dots [17] are relatively stable against external perturbations due to the fact that the electrons in one dimension cannot exchange their positions. In circular 2D quantum dots at low carrier densities the electron localization acquires a molecular form [18, 19] only in the inner coordinates of the system and not in the charge density which remains rotationally invariant. The Wigner form of the electron density with separate single-electron islands can be observed in the laboratory frame of quantum dots of lower symmetry only for some N , for which the classical [20] charge distribution reproduces the symmetry of the confinement potential [21].

So far, the scanning gate microscopy experiments on closed two-dimensional (2D) quantum dots defined within the two-dimensional electron gas (2DEG) concerned: imaging of the single-electron quantum dot [6], mapping the position of floating double dot defined electrostatically [8], and determination of the effective tip potential as seen by the confined electrons [13]. In the present paper we consider an extent to which the energy variation induced by the tip can be used for visualization of few-electron charge density in 2D quantum dots. We investigate the relation between the Wigner molecule formation in the laboratory frame and the reaction of the confined density on the potential of the tip. We perform configuration interaction calculations taking into account both the electron-electron correlation and the reaction of the quantum dot to

the tip potential. The study covers up to four electrons and quantum dots of various symmetries and profiles. We discuss the adequacy of the perturbative approach for extraction of the electron density [6, 11, 12] confined in quantum dots and the fidelity of charge images outside the perturbative regime. We find that the images obtained with repulsive (attractive) tip potential tend to overestimate (underestimate) the electron localization. We demonstrate that the confined charge density is best resolved when the classical electron configuration agrees with the symmetry of the confinement potential. We also identify cases when the confined electron density evades visualization even for weak perturbation introduced by the tip.

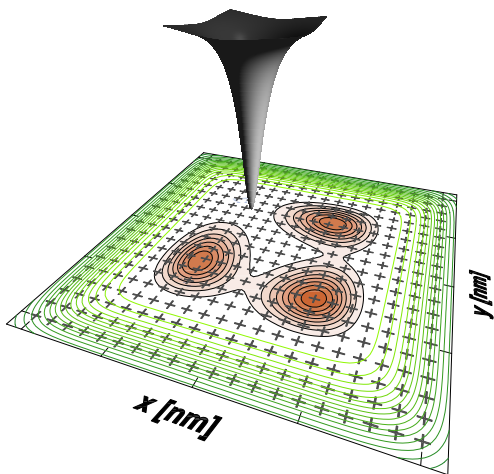


Figure 1. Schematic drawing of the considered system with the tip potential perturbing the charge density (brown contour plot) of a two-dimensional quantum dot. The green contours correspond to equipotential lines. The crosses correspond to centers of Gaussians defining the multicenter basis given by Eq. (3).

2. Theory

In this work we assume a strictly two-dimensional model of confinement which is usually justified by the strong confinement of 2DEG in the growth direction (z). The Hamiltonian of N -electron system is taken in form

$$H = \sum_i^N h(\mathbf{r}_i) + \frac{e^2}{4\pi\epsilon\epsilon_0} \sum_{i=1}^N \sum_{j=i+1}^N \frac{1}{r_{ij}}, \quad (1)$$

where \mathbf{r}_i is the position of the i th electron and h is the single-electron Hamiltonian,

$$h = -\frac{\hbar^2}{2m^*} \nabla^2 + V(\mathbf{r}) + V_t(\mathbf{r}; \mathbf{r}_t). \quad (2)$$

In Eq. (2), m^* is the effective mass, ϵ is the dielectric constant (we use GaAs material parameters $m^* = 0.067m_0$, $\epsilon = 12.5$), V stands for the external potential, V_t denotes the tip potential as seen by the electrons within the plane of confinement and \mathbf{r}_t is the position of the tip.

The single-electron eigenequation is diagonalized ($\hbar\phi_n = \epsilon_n\phi_n$) using a basis of Gaussian functions

$$\phi_n(x, y) = \sum_{k=1}^{M \times K} c_k^{(n)} \sqrt{\frac{2a}{\pi}} \exp\left(-a \left[(x - X_k)^2 + (y - Y_k)^2\right]\right), \quad (3)$$

where the centers of Gaussians (X_k, Y_k) are distributed on a rectangular lattice of $M \times K$ points (typically several hundred centers are taken – see for instance the crosses in Fig. 1) and a is optimized variationally [22]. The applied multicenter Gaussian basis allows for description of any smooth potential with arbitrary or no symmetry [22]. The few-electron eigenproblem is solved with the configuration interaction approach using the eigenstates of operator (2) for construction of the basis. The single-electron eigenfunctions (ϕ_n) are used for construction of Slater determinants that are used as the basis for the N -electron Schrödinger equation for Hamiltonian (1),

$$\Psi(\{x_i, y_i, \sigma_i; i = 1, \dots, N\}) = \sum_k d_k \mathcal{A}[\phi_{k1}(x_1, y_1)\chi_{k1}(\sigma_1) \dots \phi_{kN}(x_N, y_N)\chi_{kN}(\sigma_N)], \quad (4)$$

where \mathcal{A} is the antisymmetrization operator, and χ_k is one of the eigenstates of the spin Pauli σ_z matrix. For construction of the basis of determinants we use up to 38 single-electron spin-orbitals.

In experiment the maps of the chemical potential $\mu_N(x_t, y_t) = E_N - E_{N-1}$ can be gathered by re-tuning the conditions for the current flow (i.e. lifting of the Coulomb blockade) with varied backgate potential or bias. Since $\mu_1 = E_1$, the energy maps as functions of the tip position can be deduced for any N . Simulation of the confined charge density mapping by the SGM technique is performed in the following sequence. We first calculate the energy of N -electron system as a function of the tip position. The charge density extracted from the energy map n_r is obtained under the assumption that the action of the tip is perturbative [6, 11, 12]

$$E_N(\mathbf{r}_t) = E_N(\infty) + \int_{-\infty}^{\infty} \int_{-\infty}^{\infty} dx dy V_t(\mathbf{r}; \mathbf{r}_t) n_r(\mathbf{r}). \quad (5)$$

Equation (5) is a convolution of the tip potential and the confined charge density. The charge density can be extracted from the energy dependence of the tip position using the Fourier transform technique [6, 11]. Alternatively Eq. (5) can be treated as the Fredholm-type integral equation for n_r . We apply the Nyström approach replacing the integral by a quadrature (rectangle rule). Upon replacement we obtain a linear system of equations for the charge density in the mesh points used for the quadrature. In the following we compare the charge density deduced in this way (n_r) with the exact one (n) that is calculated from the few-electron wave function

$$n(\mathbf{r}) = \langle \Psi | \sum_{i=1}^N \delta(\mathbf{r} - \mathbf{r}_i) | \Psi \rangle. \quad (6)$$

For comparison we calculate also the charge density n_δ assuming that the tip potential is point-like $V_p = V_T \delta(x - x_t, y - y_t)$. Then, Eq. (5) reduces to

$$E_N(\mathbf{r}_t) = E_N(\infty) + V_T n_\delta(\mathbf{r}_t). \quad (7)$$

Normalized charge density n_δ derived from this formula is simply proportional to the energy variation.

The original potential of the charged tip is of the Coulomb form. As the tip approaches the 2DEG its charge density reacts by deformation which results in the screening of the tip potential. Previous Schrödinger-Poisson calculations [23] for the reaction of the 2DEG to the tip indicated that the effective (i.e. screened) tip potential is close to the Lorentz form

$$V_t(\mathbf{r}; \mathbf{r}_t) = \frac{V_T}{\frac{(x-x_t)^2}{d_{tip}^2} + \frac{(y-y_t)^2}{d_{tip}^2} + 1}, \quad (8)$$

where the width of the tip d_{tip} turns out to be of the order of the tip – 2DEG distance [23] independent of the charge at the tip and the density of 2DEG, which only influence the strength of the perturbation V_T and not its range. The Lorentz form of the effective tip potential for SGM measurements on 2DEG was also found in experimental studies of 2D quantum dots [13]. Therefore, in the bulk of this work we use mainly the Lorentz model potential of the tip and assume $d_{tip} = 20$ nm, which seems the smallest reasonable value of the potential width. For comparison we also consider the reaction of the confined system to the long-range Coulomb potential

$$V_t^c(\mathbf{r}; \mathbf{r}_t) = \frac{Qe}{4\pi\epsilon\epsilon_0} \frac{1}{\left((x - x_t)^2 + (y - y_t)^2 + z_{tip}^2\right)^{1/2}}, \quad (9)$$

where Q is the tip potential, and z_{tip} – the position of the tip above the 2DEG plane.

An ample discussion of potentials of electrostatic quantum dots defined within 2DEG was given in Ref. [24]. The calculations [24] indicated that depending on the geometry of the device one can obtain both parabolic and quantum well profiles. The latter can only be realized for large dots [24] of the linear extent of the order of a few hundred nm, i.e. the ones which are studied in the present work. Since our purpose is to determine the relation between the N –dependent classical electron distribution and the quantum dot geometry we consider a number of potentials: parabolic

$$V(x, y) = \frac{m}{2} (\omega_x^2 x^2 + \omega_y^2 y^2), \quad (10)$$

of circular $\omega_x = \omega_y = \omega$ and elliptic $\omega_x \neq \omega_y$ symmetry, as well as non-parabolic dots modeled by formula

$$V(x, y) = V_0 \left(1 - \frac{1}{1 + (\frac{x}{X})^{10} + (\frac{y}{Y})^{10}} \right) \quad (11)$$

which produces a well-like potential with a flat bottom of a nearly rectangular shape of dimensions $2X \times 2Y$. For Eq. (11) we discuss the dots from a nearly 1D ($X \gg Y$) to square ($X = Y$) geometry.

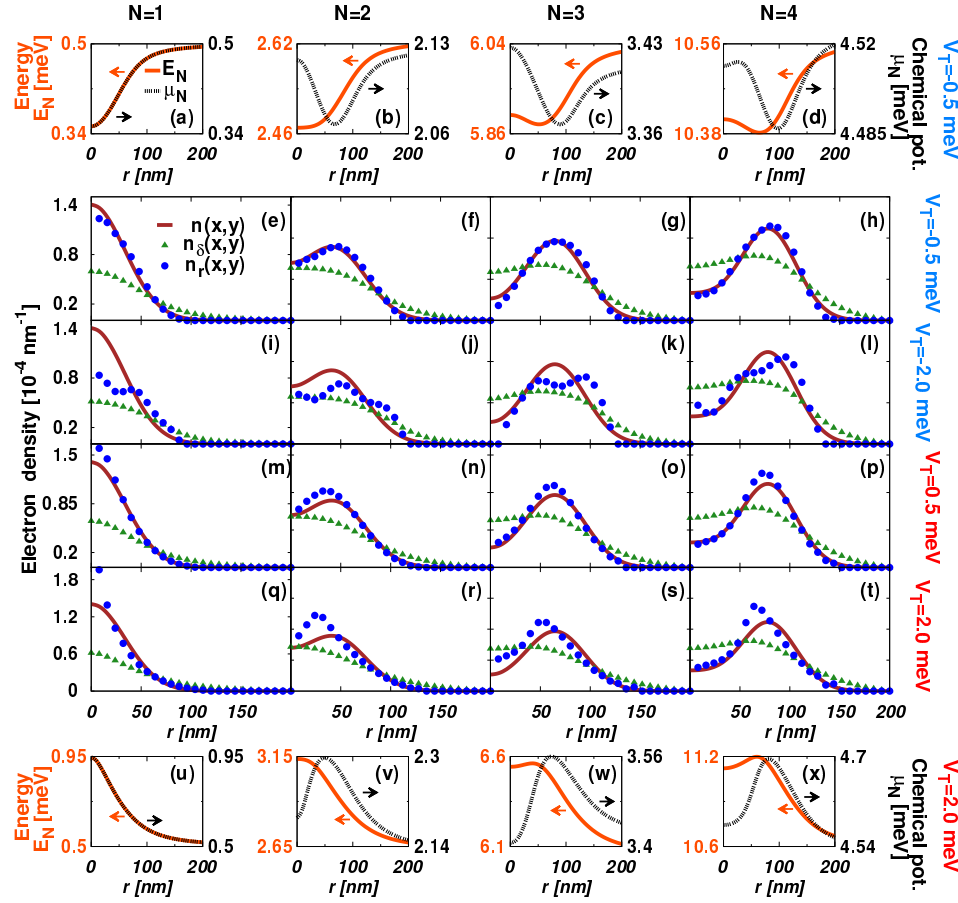


Figure 2. Results for a circular harmonic oscillator potential with $\hbar\omega = 0.5$ meV and the potential of the tip of the Lorentz form [Eq.(8) with $d_{tip} = 20$ nm]. The columns correspond to various electron number from $N = 1$ to 4. The first (last) row of plots shows the energies and chemical potentials for $V_T = -0.5$ meV ($V_T = 2$ meV). The rows from the second (e-h) to the fifth (q-t) show the electron densities: the unperturbed one (n brown solid lines), the one reproduced with the perturbative formula (5) (n_r , blue dots) and the one obtained under assumption of a delta-like perturbation (n_δ , green triangles). Subsequent rows correspond to various values of V_T .

3. Results and Discussion

3.1. Circular potential

Let us first consider a circular parabolic quantum dot with $\hbar\omega = 0.5$ meV. The solid line in Fig. 2(e,f,g,h) shows the unperturbed radial charge density for 1,2,3 and 4 electrons, respectively. When a tip modeled by the attractive Lorentzian with $V_t = -0.5$ meV moves above the system, the changes in the energy are of the order of 0.2 meV only [Fig. 2(a-d)]. The reproduced charge density: n_r (circles) very well agrees with the unperturbed density, which is also the case for weak repulsive tip potential [Fig. 2(m-p)]. A stronger amplitude of the energy variation should be useful for the signal to noise ratio of the experimental maps. For a stronger attractive perturbation ($V_t = -2$

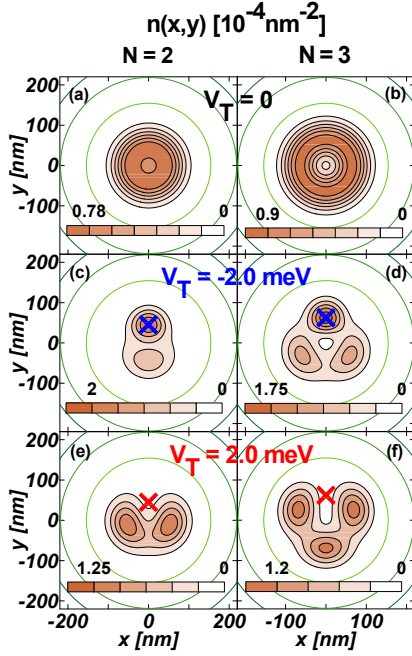


Figure 3. Charge densities for $N = 2$ and 3 electrons for parameters of Fig. 2. The cross marks the tip position. The solid green curves show the equipotential lines.

meV, Fig. 2(i-l)) we notice that the size of the charge droplet is overestimated with an extra oscillation of a small amplitude. On the other hand: a stronger repulsive potential ($V_t = 2$ meV, Fig. 2(q-t)) gives a smaller size of the droplet.

Figure 3 shows the two- and three- electron densities: unperturbed [Fig. 3(a-b)], and in the presence of the tip [Fig. 3(c-f)]. The attractive tip $V_t = -2$ meV captures a part of the density underneath [Fig. 3(c-d)], the position of the other electron islands becomes well resolved. The repulsive tip also pins the orientation of the Wigner molecule in the laboratory frame [Fig. 3(e-f)], only with a void under the tip position. The impact of the tip on the electron density is therefore a drastic one for both negative and positive tip potentials, so a success of the perturbative formula given by Eq. (5) for reproduction of the radial density as calculated in the absence of the tip found in Fig. 2 is quite remarkable, even if the original density lacks finer details.

3.2. Elliptic potential

The finer details of the unperturbed electron density appear for dots of lowered symmetry: see the results for an elliptic ($\hbar\omega_x = 0.8$ meV, $\omega_y = 1.2\omega_x$) quantum dot in Fig. 4. For two electrons: single-electron islands are formed [Fig. 4(b)] along the x axis, as in the classical solution [Fig. 5(a)]. For three electrons two equivalent classical charge distributions exist [see Fig. 5(b)] each of the symmetry lower than the elliptical one, and in consequence the single-electron islands do not appear in the laboratory frame of the quantum system [Fig. 4(c)]. For each N , similarly as for the circular potential, for

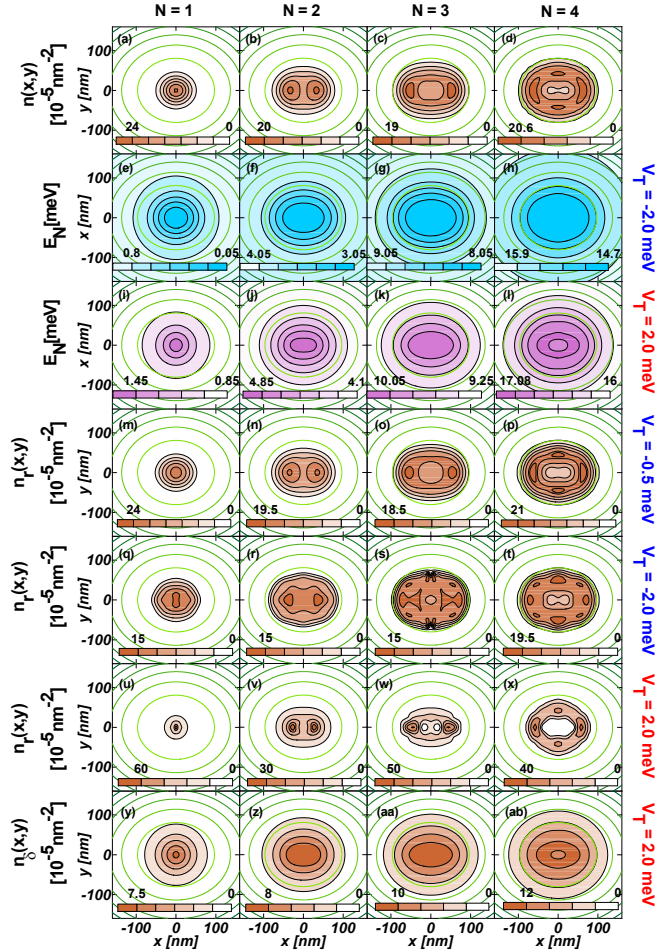


Figure 4. Results for elliptic parabolic potential with $\hbar\omega_x = 0.8$ meV, $\omega_y = 1.2\omega_x$, and the potential of the tip of the Lorentz form [Eq.(8) with $d_{tip} = 20$ nm]. Columns correspond to various electron numbers. The first row of plots (a-d) shows the charge density in the absence of the tip. Second (e-h) and third (i-l) rows show the energies in function of the tip position for $V_t = -2$ meV and $V_t = 2$ meV, respectively. Three next rows show the charge density reproduced by the perturbative formula, and the last one the density calculated for the assumption of the point-like tip potential.

a weak perturbation both negative tip [$V_t = -0.5$ meV – Fig. 4(m-p)] and positive tip [not shown], n_r density very well reproduces the unperturbed one.

Second and third rows of Fig. 4 show the energy of the system in function of the tip position for stronger attractive and repulsive tip potentials $V_T = \pm 2$ meV. For the negative tip we obtain a flat minimum, within more or less the entire region occupied by the unperturbed charge density [Fig. 4(e-h)]. The minimum appears since the tip creates its own potential minimum and the electron system follows the minimum as the tip is translated. The reproduced density [Fig. 4(q-t)] occupies larger space than the original one (as in the circular for $V_t = -2$ meV – see Fig. 2(i-l)), and a variation of

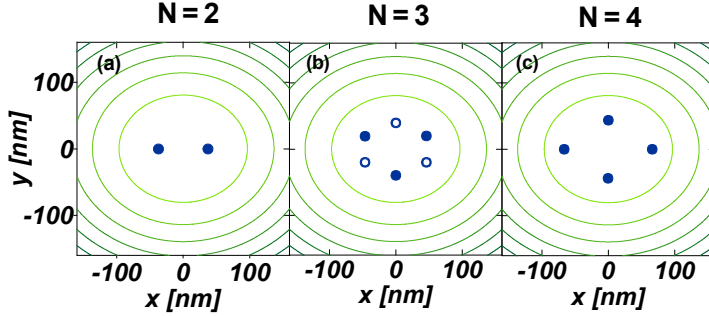


Figure 5. Classical lowest energy configurations of point charges for the elliptic potential of Fig. 4. For $N = 3$ two equivalent configurations exist which are marked by solid and empty circles, respectively.

smaller amplitude appears within the maximal density area.

For the positive tip the energy maximum is more strongly localized [Fig. 4 (i-l)] around the center of the dot, and the amplitude of n_r variation [Fig. 4 (u-x)] is drastically increased with respect to n . Also, the reproduced density occupies visibly smaller area than the original one. Nevertheless, the configuration of the maxima of n_r agrees with the ones present for n .

For $V_T = 2$ meV, the density n_δ reproduced with the assumption that the energy map – obtained in fact for the Lorentz function – is due to the delta-like tip potential, gives a closer [Fig. 4 (y-ab)] idea about the size of the charge droplet. Nevertheless, the details of the density maxima are not reproduced by n_δ .

3.3. Square quantum dot

Let us now consider a square quantum dot [confinement potential given by Eq. (11) for $X = Y = 200$ nm]. For $N > 1$ the unperturbed electron density distinctly sticks to the corners of the square dot [Fig. 6(b-d)] as should be expected for interacting charge density within a box. For $N = 2$ and 3 an increase of the density along the dot edges is also observed. The classical system of 4 electrons possesses a single lowest-energy configuration [Fig. 7(d)] which coincides with the charge density of Fig. 6(d). Systems of two and three electrons possess two and four equivalent configurations, respectively [Fig. 7(a-c)]. The few-electron wave function contains contributions of all these configurations. Since one or two corners of the square are unoccupied in the classical configurations, the lower amplitude of the maxima at the corners than in the

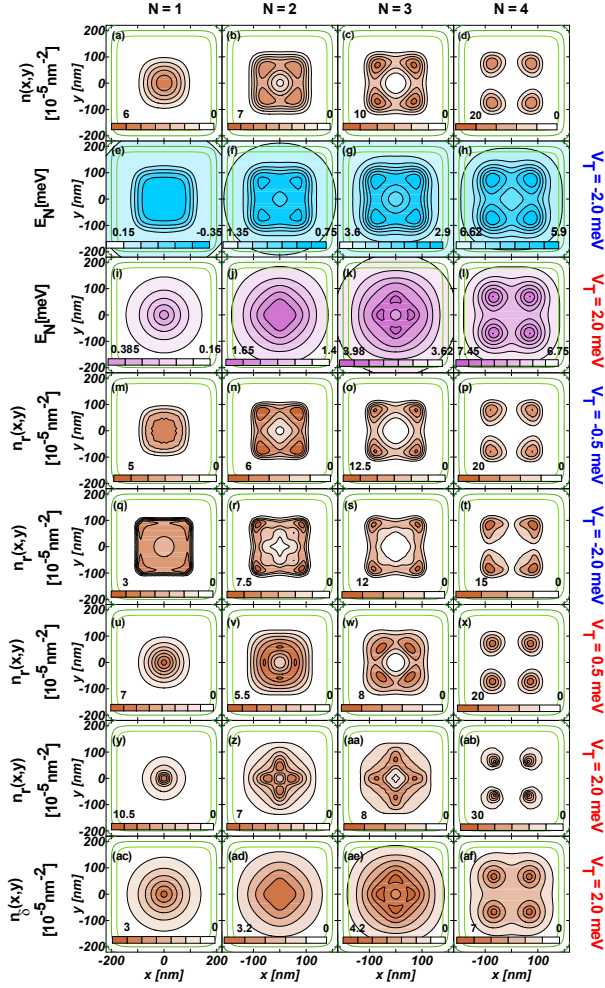


Figure 6. Results for a square quantum dot $X = Y = 200$ nm [Eq. (11)] and the tip potential the Lorentz form [Eq.(8) with $d_{tip} = 20$ nm]. Columns correspond to various electron numbers. The first row of plots (a-d) shows the charge density in the absence of the tip. Second (e-h) and third (i-l) rows show the energies in function of the tip position for $V_t = -2$ meV and $V_t = 2$ meV, respectively. Three next rows show the charge density reproduced by the perturbative formula, and the last one – the density calculated for the assumption of the point-like tip potential.

case of $N = 4$. As the negative tip scans the dot [Fig. 6(e-h)] we observe a rather flat dependence of the energy on the tip position with minima at the corners – where the unperturbed electron density is the largest. Remarkably, for the positive tip and $N = 2$ and $N = 3$ the energy extrema lie on the axes of the dot [Fig. 6(j-k)], and not on the corners. The reason for this behavior is given in Fig.8 which displays the charge distribution when the tip is present. When the tip is above the corner of the dot [Fig. 8(g-h)] we can see that the electron density becomes nearly identical with the classical systems of electrons [cf. Fig. 7(a-c)]. The other equivalent lowest-energy configurations of the charge density were excluded by the presence of the tip above one of the corners.

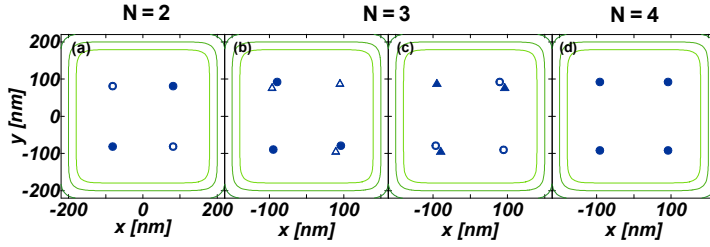


Figure 7. Classical lowest energy configurations of point charges for the potential of Fig. 6. For $N = 2$ (a) two equivalent configurations exist which are marked by different symbols. For $N = 3$ four equivalent configurations appear (b,c).

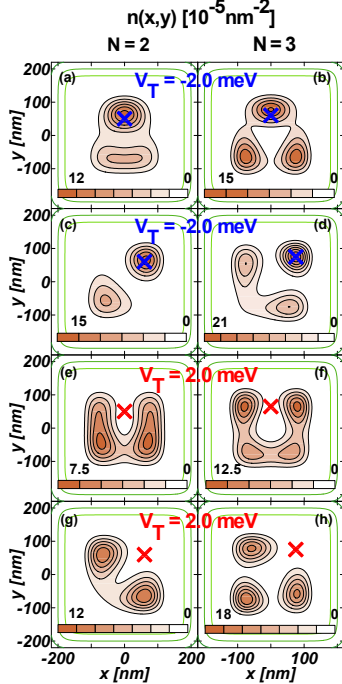


Figure 8. Charge densities for $N = 2$ and 3 electrons for parameters of Fig. 6. The cross marks the tip position.

On the other hand, for two-electrons when the tip is above the center of the side of the dot [Fig. 8(e)] the electrons instead of occupying the opposite corners of the dot,

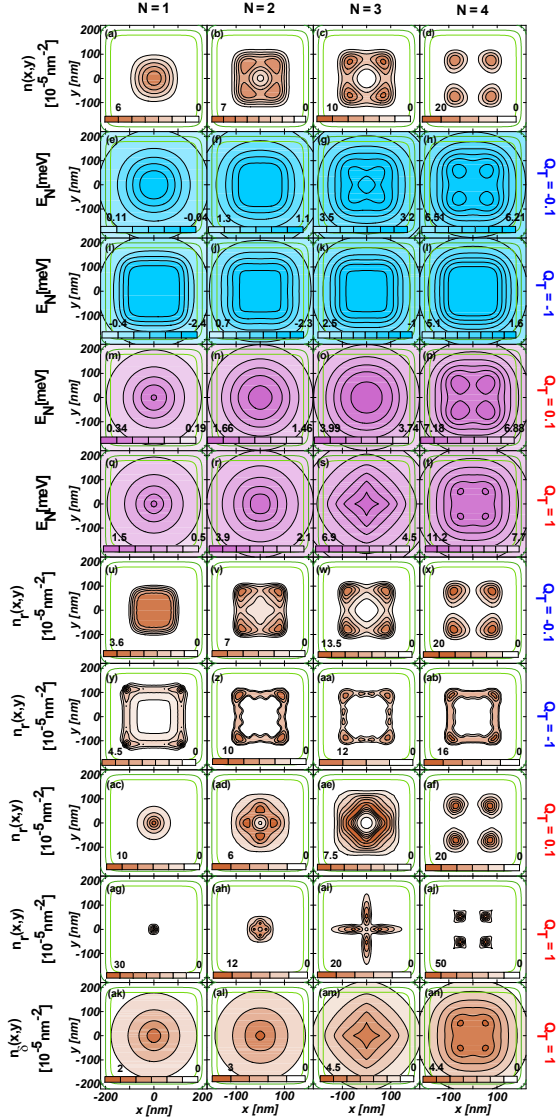


Figure 9. Results for the square quantum dot $X = Y = 200$ nm [Eq. (11)] and the tip potential the Coulomb form [Eq.(9) with $z_{tip} = 30$ nm, $Q = \pm 0.1e$ and $Q = \pm 1e$]. Columns correspond to various electron numbers. The first row of plots (a-d) shows the charge density in the absence of the tip. Plots (e-t) show the energies as functions of the tip position. Four next rows show the charge density reproduced by the perturbative formula, and the last one – the density calculated for the assumption of the point-like tip potential.

go to its other side and approach each other, hence the corresponding maximum of the energy [Fig. 6(j)]. For three electrons, formation of four instead of three charge maxima is found [Fig. 8(f)] which also increases the electrostatic energy of the system above the minimal one.

The charge density n_r as reproduced for the negative tip [Fig. 6(m-t)] exhibits maxima near the maxima of n . For stronger tip potential [Fig. 6(q-t)] the charge

density localization near the potential edges is overestimated. When a weak positive tip potential ($V_T = 0.5$ meV) is applied [Fig. 6(u-v)] we notice that the maxima are pushed to the interior of the dot from the edges. We also notice for two-electrons [Fig. 6(v)] that the position of the n_r maxima is shifted to the axes of the dot, which is the result of the energy increase for the tip above the sides of the dot discussed above. For $V_T = 2$ meV we notice a similar phenomenon also for three electrons [Fig. 6(aa)]. For one and four electrons [Fig. 6(y,ab)] the maxima are localized in the correct positions, and they distinctly shrink in size as compared to the maxima of n .

We also considered the mapping of the charge density confined in the square quantum dot by the long-range Coulomb potential [Eq. (9)] i.e. for neglected screening of tip potential – see Fig. 9. We considered the tip localized $z_{tip} = 30$ nm above the dot and the charge at the tip $Q = \pm 1$ and ± 0.1 [e], for which the maximal value of the perturbation below the tip equals 3.8 meV and 0.38 meV, respectively. The weak ($Q = -0.1$) attractive perturbation [Fig. 9(u-x)] gives n_r which well agree with n . On the other hand already for the weak repulsive perturbation ($Q = 0.1$) the maxima of n_r for $N = 2$ and 3 go to the axes of the dot – the phenomenon observed above for the Lorentz perturbation. For $Q = \pm 1$ the calculated n_r differs drastically from the unperturbed density n . For $Q = -1$, n_r [Fig. 9(y-ab)] drifts to the edges of the dot. This density localization convolved [Eq. (5)] with the Coulomb potential gives the flat energy curve of Fig. 9(i-l). On the other hand for the positive potential $Q = 1$ the derived n_r density [Fig. 9(ag-aj)] is localized in tiny islands inside the dot and only for a single and four electrons – for which a single classical configuration of the charge exists – their positions are close to the original ones. For $N = 2$ and $N = 3$ the switching between similar configurations of the type presented in Fig. 8 becomes so strong, that the reproduced charge density [Fig. 9(ah,ai)] have little in common with the original one.

3.4. Rectangular quantum dot near 1D limit

Finally, let us consider the rectangular quantum dot near the 1D limit ($X = 250$ nm, $Y = 50$ nm). The results for the Lorentz and Coulomb tip potentials are displayed in Figs. 10 and 11, respectively. For this dot the classical few-electron systems for $N = 2, 3, 4$ possess two equivalent zig-zag configurations [Fig. 12]. The electron positions in the two configurations differ only slightly and these differences are not resolved in the quantum charge density, which presents well resolved single-electron islands that are clearly visible in the original electron density for all N [Fig. 10(a-d)]. The single-electron islands are also well resolved in the maps obtained for all the Lorentz tip potentials considered in Fig. 10(m-x), as well as in the crudest assumption of point-like potential [Fig. 10(y-ab)]. The charge density islands obtained for $V_T = -2$ meV [Fig. 10(q-t)] are distinctly more extended along the axis of the dot, which results from the fact that the islands follow the attractive tip as it moves. On the other hand for $V_T = 2$ meV [Fig. 10(u-x)] an extension of the n_r densities in the direction perpendicular to

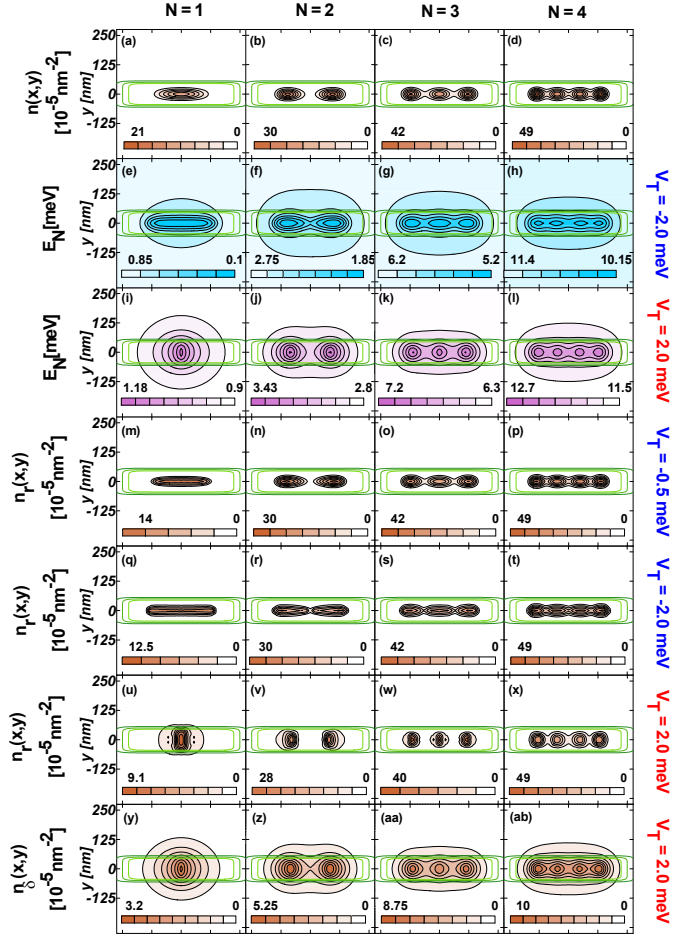


Figure 10. Results for the rectangular quantum dot $X = 250\text{nm}$, $Y = 50\text{ nm}$ [Eq. (11)] and the tip potential the Lorentz form [Eq.(8) with $d_{tip} = 20\text{ nm}$]. Columns correspond to various electron numbers. The first row of plots (a-d) shows the charge density in the absence of the tip. Second (e-h) and third (i-l) rows of plots show the energies as functions of the tip position. Three next rows show the charge density reproduced by the perturbative formula, and the last one – the density calculated for the assumption of the point-like tip potential.

the axis is found. When the repulsive tip localized near the edges of the dot its width in y direction is effectively reduced. In this way the tip increases not only the local potential energy but also the kinetic energy due to the localization. For that reason, the perturbative formula produces the charge density which penetrates the region outside the dot, where the original density vanishes.

The repulsive Coulomb potential reproduces correctly the charge localization [Fig. 11(q-t)] with an enhanced effect of the elongation of charge density island perpendicular to the dot. On the other hand, the attractive Coulomb potential [Fig. 11(m-p)] misses the details of the charge density which is seen as equally spread along the dot. For $Q = \pm 0.1$ (not shown) the 1D Wigner molecule is well reproduced by n_r .

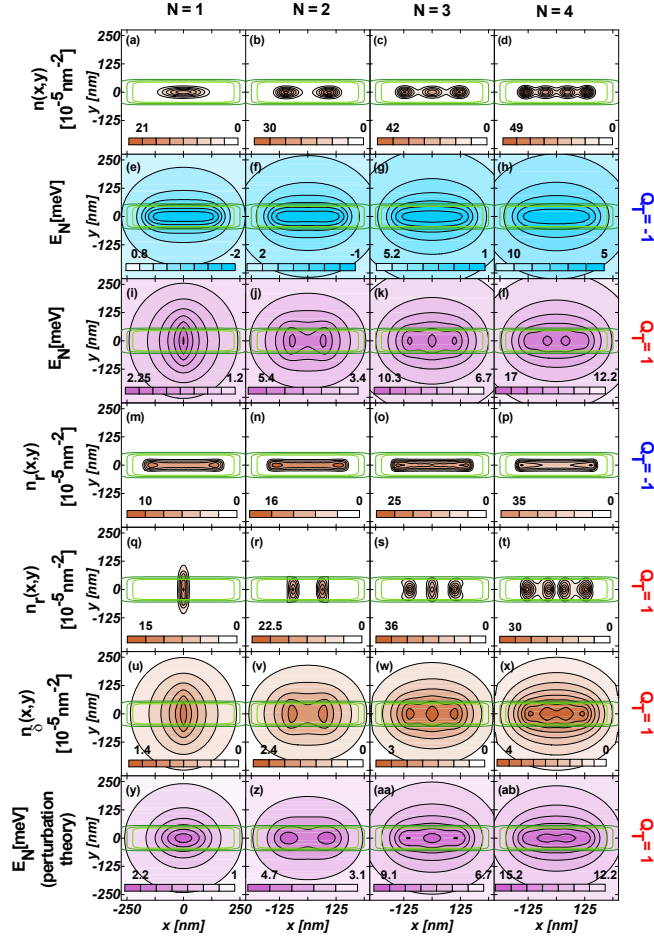


Figure 11. Same as Fig. 10 only for the tip potential of the Coulomb form [Eq.(9)] with $z_{tip} = 30$ nm, $Q = \pm 0.1$ [e] and $Q = \pm 1$ [e].

4. Summary and Conclusions

We have performed simulations of the charge density mapping for electron systems confined in two-dimensional quantum dots using model tip potentials of the Lorentz and Coulomb form, several confinement potentials and the exact solution of the few-electron Schrödinger equation. We investigated large quantum dots, where the electron-electron correlation is strong, which can give rise to formation of single-electron islands in the laboratory frame, i.e. the Wigner molecules.

For the circular dots we found that the molecular electron distributions appear in the laboratory frame pinned by the tip potential. The Wigner molecule follows the tip as it moves above the dot. In consequence the energy map in function of the tip position is rotationally invariant, and the density map reproduced by the perturbative formula is very close to the original one. We noticed that a stronger repulsive (attractive) tip leads to underestimate (overestimate) of the charge density size. This conclusions for the size of the droplet holds for any dot profile studied. Moreover, for the elliptical

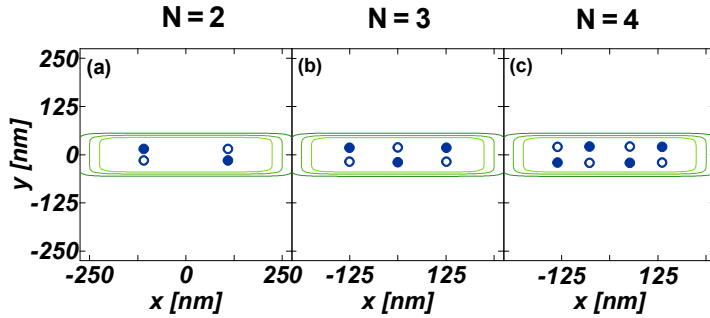


Figure 12. Classical lowest energy configurations of point charges for the potential of Fig. 10. For each N considered two equivalent configurations appear.

and square quantum dots single-electron islands appear in the charge density for some N , and they are resolved in the charge density that is reproduced from the integral perturbative formula. We have found that in the 1D dots the Wigner molecule is clearly visible in the charge density mapped from the energy dependence for all N and for most of the tip potential studied, with the exception of the negative Coulomb potential for which the single-electron islands are lost. We demonstrated that the charge density of electron systems which possess a few equivalent classical configurations, generally are difficult to be resolved by the scanning probe technique for the repulsive tip potential, since the tip switches between equivalent configurations. In consequence, the mapped charge density maxima do not overlap with the original ones.

Acknowledgments

This work was supported by National Science Centre according to decision DEC-2012/05/B/ST3/03290 and by PL-Grid Infrastructure. Calculations were performed in ACK–CYFRONET–AGH on the RackServer Zeus.

- [1] H. Sellier, B. Hackens, M.G. Pala, F. Martins, S. Baltazar, X. Wallart, L. Desplanque, V. Bayot and S. Huant, *Sem. Sci. Tech.* **26**, 064008 (2011); D.K. Ferry, A.M. Burke, R. Akis, R. Brunner, T.E. Day, R. Meisels, F. Kuchar, J P Bird, and B R Bennett, *Sem. Sci. Tech.* **26**, 043001 (2011).
- [2] M.A. Topinka, B.J. LeRoy, S.E.J. Shaw, E.J. Heller, R.M. Westervelt, K.D. Maranowski, and A.C. Gossard, *Science* **289**, 2323 (2000); M.A. Topinka, B.J. LeRoy, R.M. Westervelt, S.E.J. Shaw, R. Fleischmann, E.J. Heller, K.D. Maranowski, A.C. Gossard, *Nature*, **410**, 183 (2001). K. E. Aidala, R.E. Parott, T. Kramer, E.J. Heller, R.M. Westervelt, M.P. Hanson, and A.C. Gossard, *Nature Physics* **3**, 464 (2007).
- [3] D.K. Ferry, R. Akis, and J. P. Bird, *Phys. Rev. Lett.* **93**, 026803 (2004); A.M. Burke, R. Akis, T.E. Day, G. Speyer, D.K. Ferry, and B.R. Bennett, *Phys. Rev. Lett.* **104**, 176801 (2010).

- [4] B. Hackens, F. Martins, T. Ouisse, H. Sellier, S. Bollaert, X. Wallart, A. Cappy, J. Chevrier, V. Bayot, and S. Huant, *Nature Physics* **2**, 826 (2006); F. Martins, B. Hackens, M. G. Pala, T. Ouisse, H. Sellier, X. Wallart, S. Bollaert, A. Cappy, J. Chevrier, V. Bayot and S. Huant, *Phys. Rev. Lett.* **99**, 136807 (2007); M. G. Pala, B. Hackens, F. Martins, H. Sellier, V. Bayot, S. Huant, and T. Ouisse, *Phys. Rev. B* **77**, 125310 (2008); M.G. Pala, S. Baltazar, F. Martins, B. Hackens, H. Sellier, T. Ouisse, V. Bayot, S. Huant, *Nanotechnology* **20**, 264021 (2009);
- [5] This technique is called Coulomb blockade microscopy by some groups [14, 15].
- [6] P. Fallahi, A.C. Bleszynski, R.M. Westervelt, J. Huang, J.D. Walls, E.J. Heller, M. Hanson, and A.C. Gossard, *Nano Lett.* **5**, 223 (2005).
- [7] L.M. Zhang and M.M. Fogler, *Nano Lett.* **6**, 2206 (2006).
- [8] A.E. Gildemeister, T. Ihn, M. Sigrist, and K. Ensslin, *Phys. Rev. B* **75**, 195338 (2007).
- [9] A. C. Bleszynski-Jayich, L. E. Fröberg, M. T. Björk, H.J. Trodahl, L. Samuelson, and R.W. Westervelt, *Phys. Rev. B* **77**, 245327 (2008).
- [10] N.T Ziani, F. Cavaliere, and M. Sassetti, *Phys. Rev. B* **86**, 125451 (2012).
- [11] E.E. Boyd and R.M. Westervelt, *Phys. Rev. B* **84**, 205308 (2011).
- [12] E.E. Boyd, K. Storm, L. Samuelson, and R.M. Westervelt, *Nanotechnology* **22**, 185201 (2011).
- [13] M. Huefner, B. Kueng, S. Schnez, K. Ensslin, T. Ihn, M. Reinwald and W. Wegscheider, *Phys. Rev. B* **83**, 235326 (2011).
- [14] D. Mantelli, F. Cavaliere, and M. Sassetti, *J. Phys. Condens. Matter* **24**, 43202 (2012).
- [15] J. Qian, B.I. Halperin, and E.J. Heller, *Phys. Rev. B* **81**, 125323 (2010).
- [16] L.P. Kouwenhoven, D.G. Austing and S. Tarucha, *Rep. Prog. Phys.* **64**, 701 (2001).
- [17] W. Hausler and B. Kramer, *Phys. Rev. B* **47**, 16353 (1993); K. Jauregui, W. Hausler, and B. Kramer, *Europhys. Lett.* **24**, 581 (1993); E. Rasanen, H. Saarikoski, V.N. Stavrou, A. Harju, M.J. Puska, and R.M. Nieminen, *Phys. Rev. B* **67**, 235307 (2003); B. Szafran, F.M. Peeters, S. Bednarek, T. Chwiej, and J. Adamowski, *Phys. Rev. B* **70**, 035401 (2004); E.J. Müller, *Phys. Rev. B* **72**, 075322 (2005); M.M. Fogler and E. Pivovarov, *Phys. Rev. B* **72**, 195344 (2005); T. Sako and G.H.F. Diercksen, *J. Phys.: Cond. Matt.* **20**, 155202 (2008); F. Malet and P. Gori-Giorgi, *Phys. Rev. Lett.* **109**, 24602 (2012); J.J. Wang, W. Li, S. Chen, X.L. Gao, M. Rontani, and M. Polini, *Phys. Rev. B* **86**, 075110 (2012); F. Malet, A. Mirtschink, J.C. Cremon, S.M. Reimann, and P. Gori-Giorgi, *Phys. Rev. B* **87**, 115146 (2013).
- [18] P.A. Maksym, *Phys. Rev. B* **53**, 10871 (1996).
- [19] S.M. Reimann and M. Manninen, *Rev. Mod. Phys.* **74**, 1283 (2002).
- [20] V.M. Bedanov and F.M. Peeters, *Phys. Rev. B* **49**, 2667 (1994).
- [21] B. Szafran, F.M. Peeters, S. Bednarek, and J. Adamowski, *Phys. Rev. B* **69**, 125344 (2004).
- [22] T. Chwiej and B. Szafran, *Phys. Rev. B* **78**, 245306 (2008).
- [23] B. Szafran, *Phys. Rev. B* **84**, 075336 (2011).
- [24] S. Bednarek, B. Szafran, K. Lis, and J. Adamowski, *Phys. Rev. B* **68**, 155333 (2003).

$$n(x,y) [10^{-5} \text{ nm}^{-2}]$$

N = 2

N = 3

